JOURNAL OF CHEMICAL INFORMATION AND MODELING

Article

pubs.acs.org/jcim

Computational Approaches Elucidate the Allosteric Mechanism of Human Aromatase Inhibition: A Novel Possible Route to Small-Molecule Regulation of CYP450s Activities?

Jacopo Sgrignani,[†,⊥] Marta Bon,[‡,⊥] Giorgio Colombo,[*,†] and Alessandra Magistrato[*,‡]

[†]Istituto di Chimica del Riconoscimento Molecolare, CNR, Via Mario Bianco 9, 20131 Milano, Milano, Italy

[‡]CNR-IOM-Democritos National Simulation Center c/o SISSA, via Bonomea 265, 34165 Trieste, Trieste, Italy

Supporting Information

ABSTRACT: Human aromatase (HA) is a P450 cytochrome (CYP) with an essential role in estrogen biosynthesis. Since more than 70% of breast cancers are positive for estrogenic receptor (ER), the reduction of estrogen physiological concentrations through HA inhibition is one of most important therapeutic strategies against this cancer type. Recently, experimental evidence showed that selected taxmoxifen metabolites, which are typically used as estrogen receptor modulators (SERMs), inhibit HA through an allosteric mechanism. In this work, we present a computational protocol to (i) characterize the structural framework and (ii) define the atomistic details of the determinants for the noncompetitive inhibition mechanism. Our calculations identify two putative binding sites able to efficiently bind all tamoxifen metabolites. Analysis of long-scale molecular dynamics simulations reveal that endoxifen, the most effective noncompetitive inhibitor, induces significant enzyme rigidity by binding in one of the possible peripheral sites. The consequence of this binding event is the suppression of one of the functional enzymatic collective motions associated with breathing of the substrate access channel. Moreover, an internal dynamics-based alignment of HA with six other human cytochromes shows that this collective motion is common to other members of the CYP450 protein family. On this basis, our findings may thus be of help for the development of new (pan)inhibitors for the therapeutic treatment of cancer, targeting and modulating the activity of HA and of estrogen receptor, and may also stimulate the development of new drug design strategies for chemoprevention and chemoprotection via allosteric inhibition of CYP450 proteins.

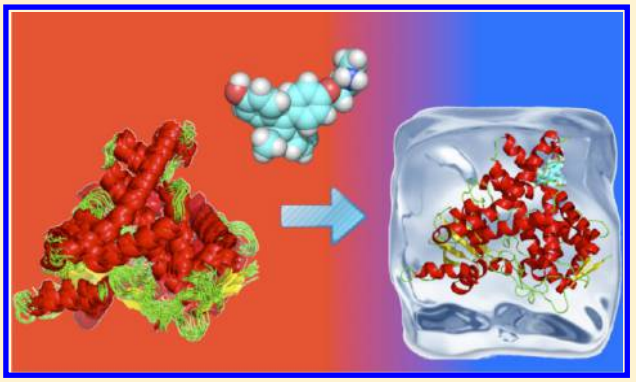

INTRODUCTION

Human Aromatase (HA) is a P450 cytochrome with a pivotal role in steroidogenesis, where it catalyzes the conversions of all androgens (androstenedione, testosterone, and 16-hydroxytestosterone) to estrogens[1,2] via three consecutive oxidative reactions, requiring molecular oxygen and electrons (the latter provided by a NADPH cytochrome reductase (CPR reductase)).[3] Estrogens are classical etiological factors for breast cancer (BC), but, over the years, they have also been related to the onset of other neoplastic pathologies such as endometrium, ovary, prostate, lung, and colon cancer.[4]

BC is the leading cause of cancer death in women,[5] and, notably, 70% of these cancers are classified as positive for estrogenic receptor (ER). Two main pharmacological strategies have been devised to fight BC: (i) preventing estrogens binding to their biological target (i.e., ER) by using antagonists such as selective estrogen receptor modulators (SERMs) and (ii) inhibiting estrogens biosynthesis by blocking HA enzymatic activity. Tamoxifen, via its active metabolite 4-hydroxytamoxifen, was the first ER antagonist introduced in therapy in the 1970s followed by other inhibitors such as toremifen and raloxifen.[4] These molecules act as antagonists of ER in breast tissue with an obvious efficacy for BC, but in other tissues they act as an ER agonist, causing deleterious and risky side effects and prompting research for the most effective drugs.

With regards to the inhibition of HA three inhibitors (AIs) are currently in clinical use (anastrazole, exemestane, and letrozole), representing the primary therapeutic option for BC therapy in postmenopausal women. These are, however, limited by resistance issues, which depend on an inefficient HA inhibition and/or on the modification of the estrogen signaling pathway.[6] Huge efforts are being devoted by the medicinal chemistry community to develop new AIs able to overcome resistance mechanisms, boosting to new effective anti BC therapies.

Traditionally, pharmaceutical research has focused on the development of competitive antagonists able to block HA activity, competing with androgens (the natural substrate) for the binding in the catalytic (ortosteric) site.[7] Recently Lu et al.[8] reported on the noncompetitive inhibition of HA exerted by

Received: July 17, 2014
Published: September 1, 2014

   dx.doi.org/10.1021/ci500425y | J. Chem. Inf. Model. 2014, 54, 2856−2868

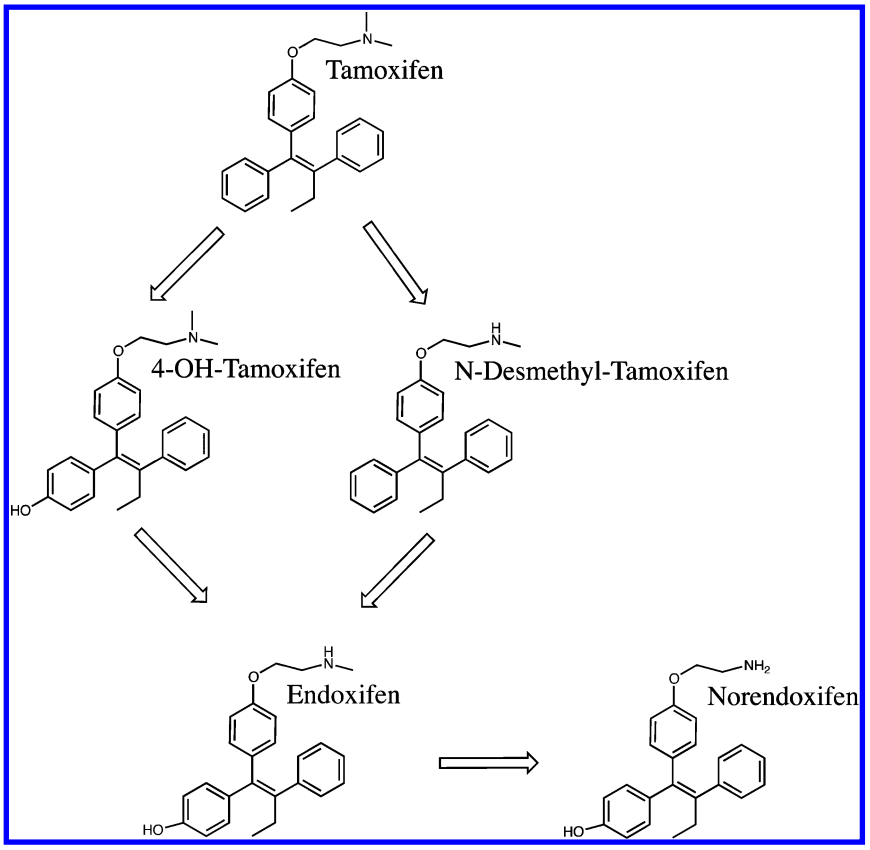

Figure 1. Schematic representation of tamoxifen metabolic pathways. Only Z stereoisomers of the drugs are shown.

Table 1. Type of Inhibition Mechanism of Tamoxifen Metabolites and Their IC50

drug	inhibition mechanism	IC_{50}
E/Z endoxifen[a]	noncompetitive	6.1 μM[8]
E/Z NDT[a]	noncompetitive	20.7 μM[8]
Z-tamoxifen		986 μM[8]
E-norendoxifen	competitive	77 ± 33 nM[10]
Z-norednoxifen	competitive	1029 ± 318 nM[10]

[a]Kinetic tests were performed using an isomeric mixture.

some tamoxifen metabolites, providing an opportunity for new possible therapeutic strategies against BC.

Among these metabolites clear evidence of noncompetitive inhibition was reported for endoxifen and *N*-desmethyl-tamoxifen (NDT),[8−10] while norendoxifen was demonstrated to be active via a competitive inhibition mechanism (Figure 1).[11] Being that tamoxifen metabolites are active as SERMs, they represent a rare case of drugs operative on two pathways associated with the same disease,[10] and they are, therefore, of particular interest for therapeutic applications.[8] To date, it is completely unclear which is (are) the allosteric site(s) targeted by noncompetitive inhibitors, and which are the molecular determinants at the basis of the HA allosteric modulation. Thus, the purpose of this work was that of gaining a detailed understanding of HA noncompetitive inhibition mechanisms, providing the first atomistic characterization drug/protein interaction with the aim of solving the previously discussed issues. Here, putative allosteric sites were identified by application of computational methods for pocket detection on the whole protein structure. Next, tamoxifen metabolites (we considered all their different isomeric forms (E/Z)) were docked into these sites, and, finally,

Table 2. Parameters for the Motion-Based Structural Alignment with HA (PDB Code 3EQM) Performed Using the ALADYN Web Server[17a]

aligned structure	identity %	RMSD	RMSIP	Z-Score	function/substrate
2HI4	16.37	2.51	0.92	12.04	drugs
1Z10	16.80	2.72	0.92	14.50	nicotine
2F9Q	15.08	2.74	0.88	11.96	drugs
1OG2	17.40	2.53	0.90	15.76	xenobiotics, drugs, environmental compounds, pollutants
1TQN	18.01	2.64	0.91	14.24	drugs
3E61	21.11	2.52	0.92	2.59	xenobiotics, fatty acids

[a]The function of each CYP is also reported.

molecular dynamics (MD) simulations of all the resulting complexes were run to optimize their structures and evaluate their relative stability. Our simulations revealed that the binding free energies of the most effective noncompetitive inhibitor endoxifen are markedly higher in one of the predicted sites. Moreover, endoxifen binding in this site alters one of the enzyme's functional collective slow motions[12] assigned to the breathing of the channel for substrate uptake/release, with clear consequences on HA catalytic activity. This finding offers new insights into the allosteric modulation of HA and possibly of other human cytochromes, which is currently the objective of several research efforts.[13−16]

Finally, an internal dynamics-based alignment[17] of HA with other CYP450 reveals the slow motion most likely associated with the noncompetitive inhibition mechanism of HA is also common to other selected CYPs. Since CYPs enzymatic function

dx.doi.org/10.1021/ci500425y | J. Chem. Inf. Model. 2014, 54, 2856−2868

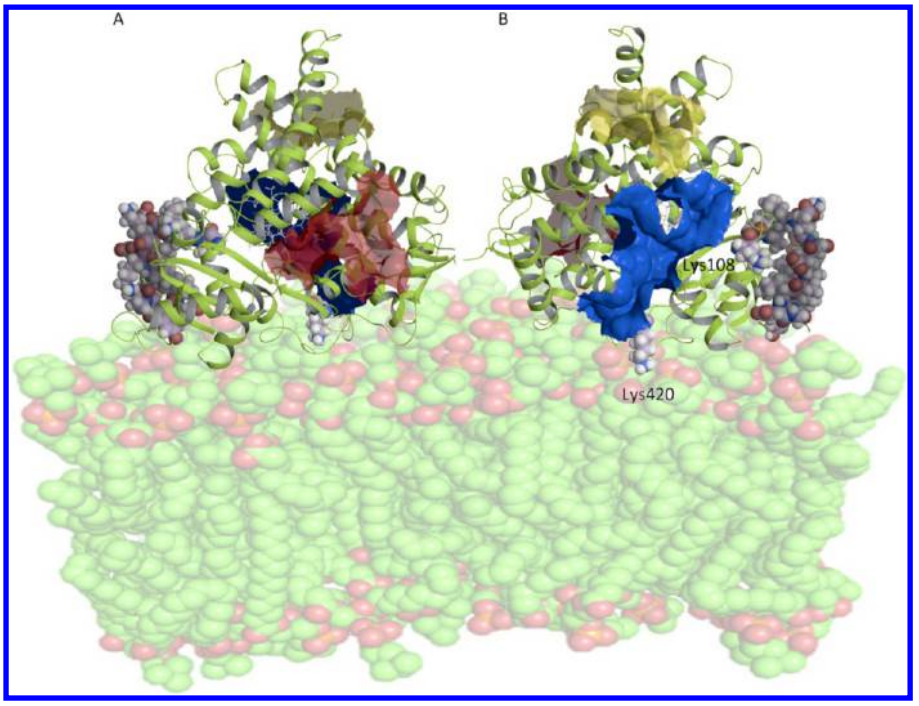

Figure 2. Putative allosteric sites predicted using SiteMap.[20,21] Site_1 is colored in red, site_2 in blue, and site_3 in yellow. Residues involved in interaction with CPR-reductase[55] are drawn as spheres. Two different protein orientations (A-B) are shown for clarity.

called as a side effect to generation of potentially carcinogenic or toxic chemicals, our work offers new general possible routes to chemoprevention or chemoprotection via regulation of CYP450s enzymatic activity.

METHODS

Identification of Putative Allosteric Sites. The HA model was built from its crystal structure (pdb code 3EQM)[18] and prepared for calculations using the "protein preparation wizard" workflow available in Maestro.[19] Possible allosteric drug-binding sites were identified using SiteMap 2.3.[20,21] This program assigns relative scores to all the mapped binding sites, ranking their ability to bind small organic molecules (additional details about SiteMap scores are available as in the Supporting Information (SI)). In this work, SiteMap analysis was carried out with the default settings. In particular, a minimum number of 15 site points were used to evaluate the propensity of each site to contribute to protein−ligand binding, considering also their proximity to the protein surface and their solvent exposure. The sites were then ranked based on their ability to bind small organic molecules with an affinity constant in the nanomolar range (see the SI). Considering a threshold of 0.9 for the SiteScore value, we considered only the 3 best sites.

Docking with Glide. Three sites (site_1, site_2, site_3) were selected to dock tamoxifen metabolites. Docking calculations were run using Glide 5.0,[22−24] and the corresponding grids were centered on the middle point of the predicted sites. Extra Precision (XP) docking mode and score were used in all the calculations. During docking calculations the HA structure was considered rigid, and induced-fit effects, due to ligand-protein interactions, were neglected. As endoxifen was identified as the most effective noncompetitive inhibitor (Table 1),[8] both its E and Z isomers were docked into the three peripheral sites. The endoxifen ligand posed with the highest GlideScore was selected for subsequent MD simulations. Docking of the other metabolites was run only on those sites in which E/Z endoxifen resulted in being stably bound during preliminary MD simulations.

Table 3. Binding ΔH, $T\Delta S$, and ΔG (kcal/mol), between the Drugs and HA Calculated over the Production Run of 100 ns Calculated with MM-PBSA and MM-GBSA[b]

	MM-PBSA	MM-GBSA		MM-PBSA	MM-GBSA
	ΔH	ΔH	$T\Delta S$	ΔG	ΔG
Site_1					
E-endoxifen	−22 (5)	−32 (4)	−21 (4)	−1 (6)	−11 (6)
Z-endoxifen	−22 (6)	−32 (6)	−20 (4)	−2 (7)	−12 (7)
E-NDT	−24 (9)	−36 (4)	−20 (7)	−4 (11)	−16 (5)
E-tamoxifen	−28 (5)	−35 (4)	−19 (6)	−9 (7)	−16 (7)
Z-tamoxifen	−31(5)	−43 (4)	−21 (6)	−10 (7)	−22 (7)
Site_3					
E-endoxifen	−25 (5)	−34 (5)	−17 (5)	−8 (7)	−17 (7)
Z-endoxifen	−28 (5)	−37 (4)	−19 (5)	−9 (7)	−18 (6)
E-NDT	−25 (4)	−35 (3)	−17 (5)	−8 (6)	−18 (6)
Z-NDT[a]	−16 (4)	−22 (5)			
E-tamoxifen	−25 (4)	−39 (3)	−18 (4)	−7 (6)	−21 (5)

[a]$T\Delta S$ and ΔG values of Z-NDT are not reported as they did not reach convergence. However, ΔH values calculated with both PB and GB are markedly less negative than the other isomers, pointing to a small ΔG. [b]Standard deviations are reported. Values of Z-NDT and Z-tamoxifen inside site_1 and site_3 are not reported because these inhibitors dissociated from HA after a few ns.

Classical MD Simulations. MD simulations were run using GROMACS 4.5.5[25] with a time step of 2.0 fs, and all bonds were constrained using LINCS.[26] Before starting the productive MD simulations, the systems were minimized for 1000 steps, using steepest descent energy minimization scheme and fixing the positions of the backbone atoms of the protein. After the minimization, one simulation of 0.2 ns was run in a NVT ensemble, freezing the coordinate of the backbone atoms and slowly increasing the temperature up to 300 K. At the end of the solvent relaxation phase, the coordinates of the backbone

dx.doi.org/10.1021/ci500425y | J. Chem. Inf. Model. 2014, 54, 2856−2868

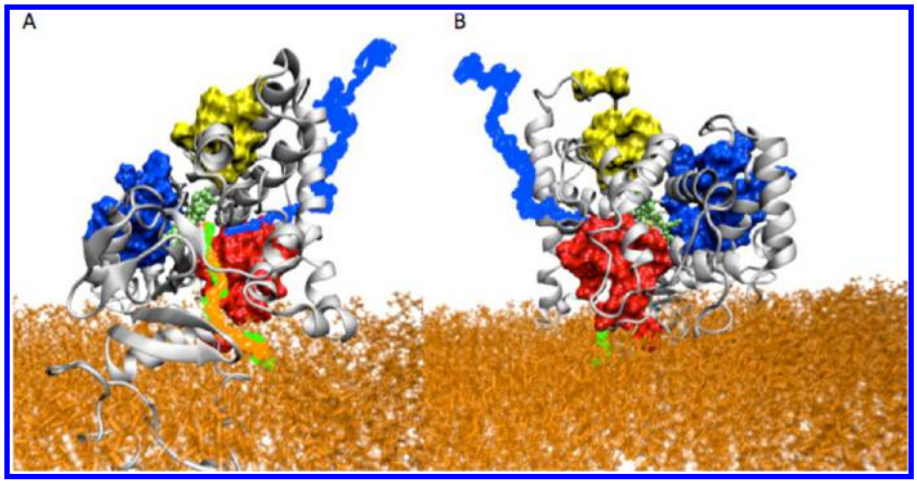

Figure 3. Positions of site_1 (red), site_2 (blue), and site_3 (yellow) relative to the three ASD entrance/exit routes identified in our previous studies[33] (blue, orange, and green lines). Two different orientations of the system (A-B) are shown for clarity.

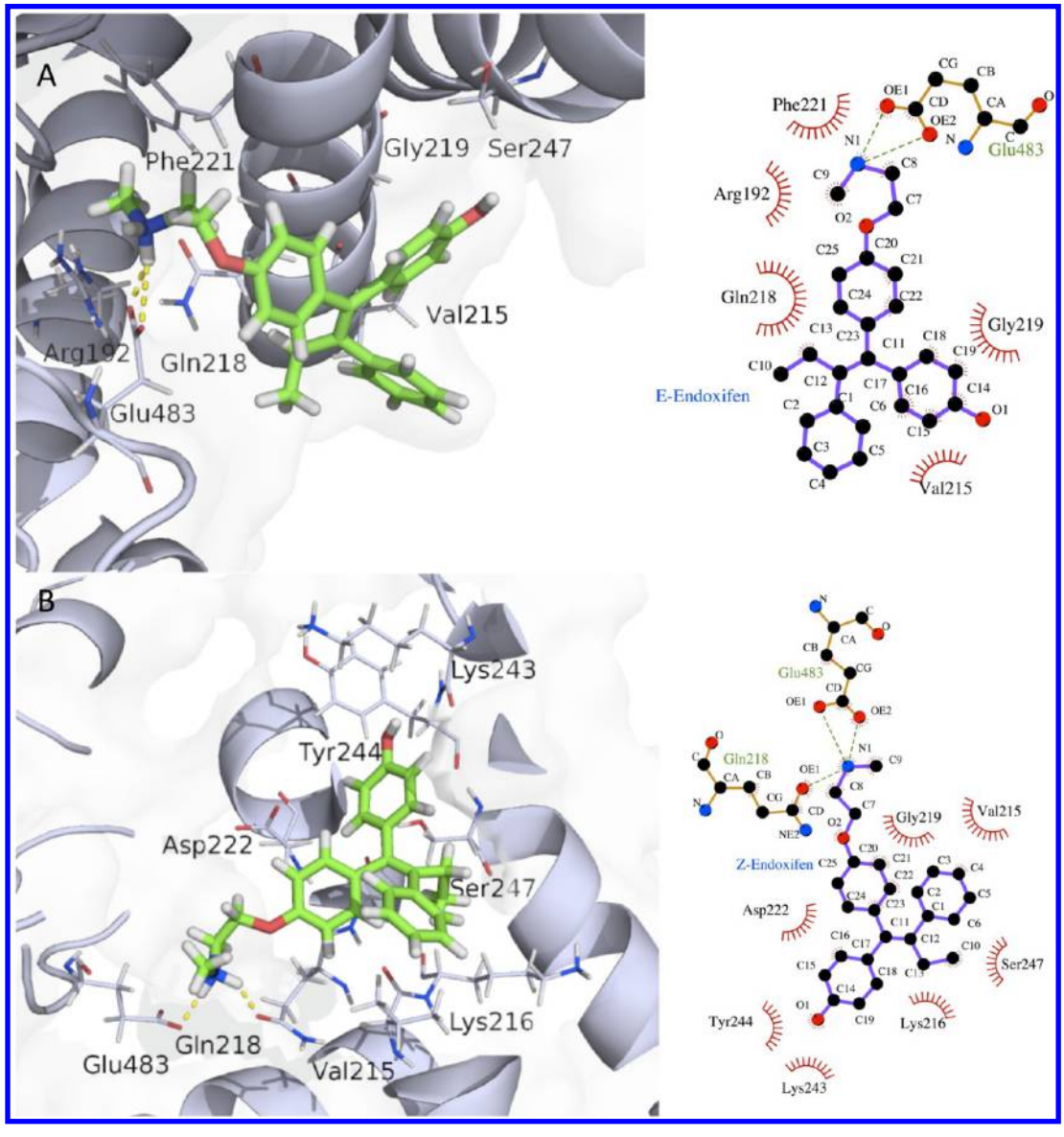

Figure 4. Three-dimensional representations and schematic plots of the interaction enstablished by E-endoxifen (A) and Z-endoxifen (B) inside site_1.

dx.doi.org/10.1021/ci500425y | J. Chem. Inf. Model. 2014, 54, 2856−2868

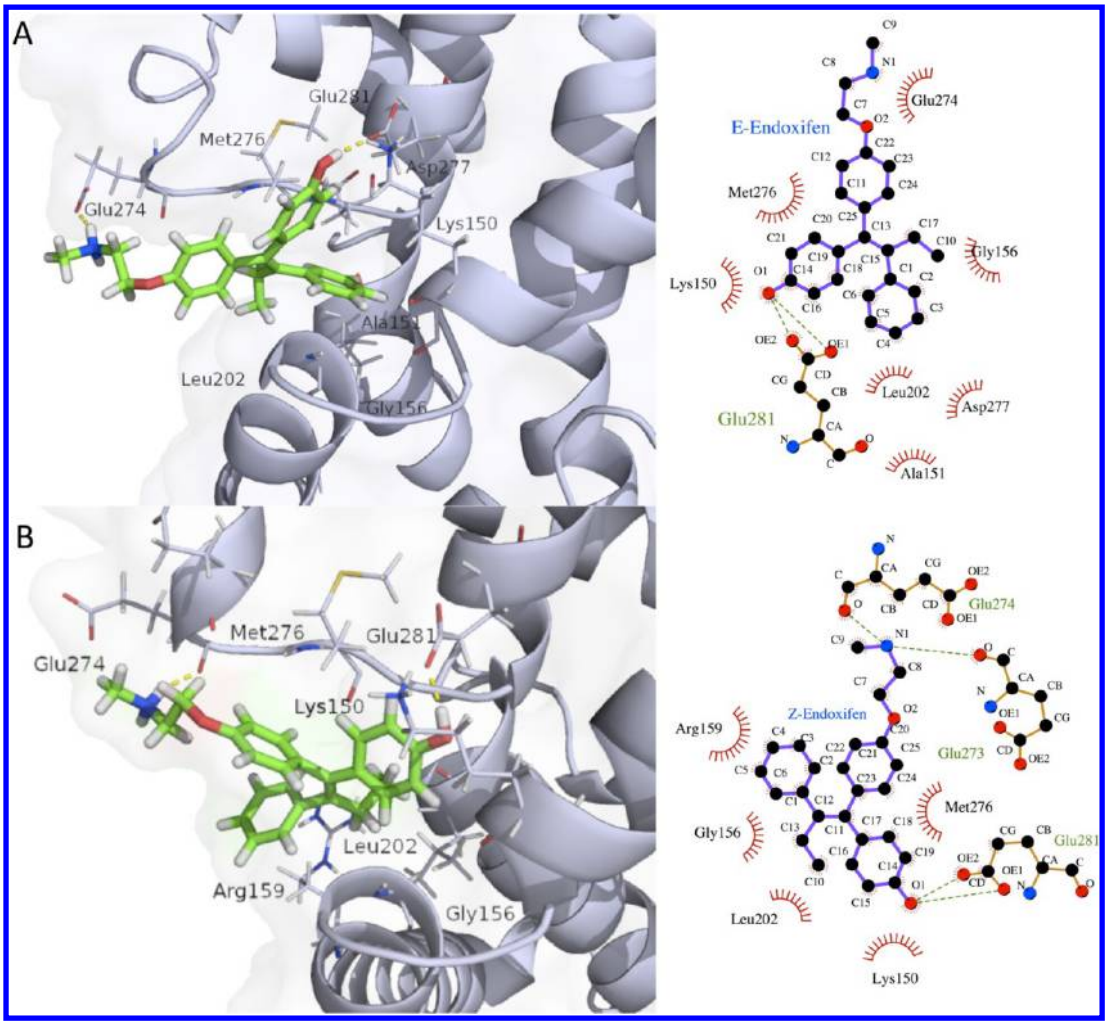

Figure 5. Three-dimensional representations and schematic plots of the interaction established by E-endoxifen (A) and Z-endoxifen (B) binding in site_3.

atoms were released, and the systems were simulated under NPT conditions for 2 ns imposing a restraint on the distance between the center of mass of the C atoms of the different drugs and the center of the C atoms of each binding site (defined considering the residues within a distance of 5 Å from the drug). In particular a distance restraint started acting on the system when the distance between the center of mass of the drug and that of the binding site was larger than 10 Å. In particular the restraint had this formulation

$$V_{\text{wall}}(s) = K\left(\frac{s - \text{LIMIT}}{\text{EPS}}\right)^{\text{exp}} \quad (1)$$

where K is an energy constant (in this case 250 kJ/mol), EPS a rescaling factor (in this case 1), and exp is the exponent determining power law (2.0). The temperature was regulated using Nosé−Hoover thermostat,[27] and the pressure was maintained to 1 bar, using Parrinello-Rahaman barostat[28] (time constant was set to 0.5 ps, compressibility was set to 4×10^{-5}1/bar). When each system was fully equilibrated (after ∼20 ns), a productive run of 100 ns was performed. Only the data sampled in production runs were considered for analyses.

All calculations were done using parm99[26] force field for the protein, the TIP3P water model for the solvent,[29] and the Åqvist parametrization for the counterions added (2 Cl^- ions) to ensure the neutrality of the system.[30] The parametrization of the heme moiety, the iron bound cysteine 437, and the iron bound oxygen molecule is the one given by Shahrokh et al. (additional details about force field performances in describing the HEME structure are available as SI),[31] while ASD, tamoxifen, and its metabolites were simulated using the general AMBER force field (gaff).[32]

According to previous computational and experimental studies[33−35] Asp309 was simulated in its neutral form. Precedent calculations revealed as HA, when embedded in a lipophilic environment, are slightly more flexible and characterized by the presence of more defined access/release channels.[33,34] However, considering the large number of drug/DNA adducts under investigation and that the membrane environment should similarly influence all systems, all the simulations were run considering only the cytosolic portion of HA immersed in a box of pure water simulated using the TIP3P model.[29]

MD Trajectory Analysis. The distances between the protein and drug center of masses as well as porcupine plots were elaborated with the tools implemented inside VMD (version 1.9.1).[36] Interaction energies were calculated with GROMACS 4.5.5. Root mean square displacements (RMSD) and root-mean-square fluctuations (RMSF) were calculated with *g_rms* and *g_rmsf*. Cluster analysis was carried out with the *g_cluster* tool on equilibrated trajectories of 100 ns. This analysis was

dx.doi.org/10.1021/ci500425y | J. Chem. Inf. Model. 2014, 54, 2856−2868

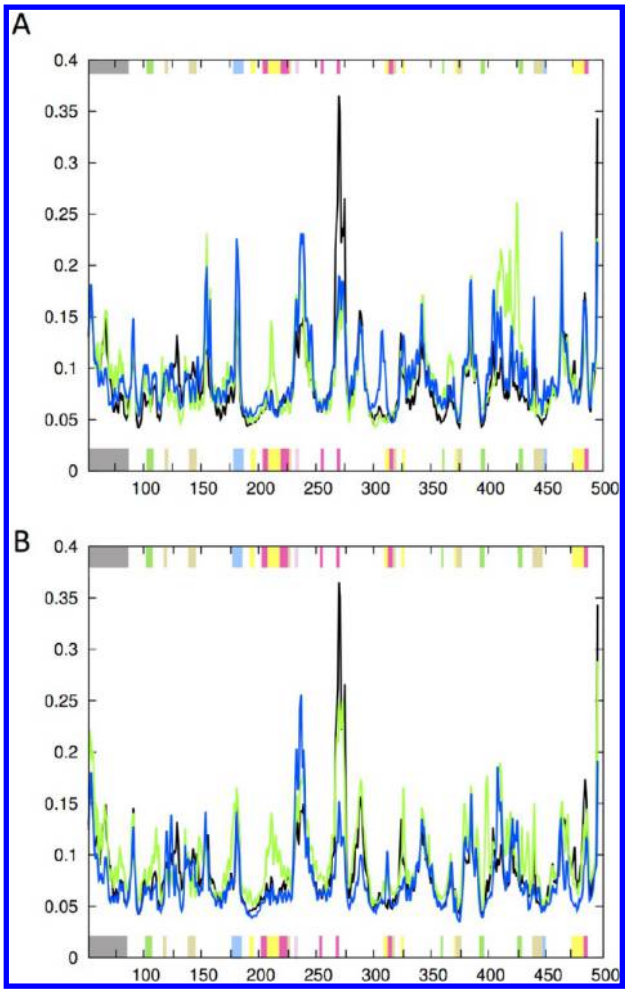

Figure 6. RMSF per residue for free HA (black line) in complex with E-endoxifen (green line) and Z-endoxifen (blue line) bound in site_1 (A) and site_3 (B). With the different colors at the top and at the bottom of the picture we indicate the zones to which key-residues (listed in Table S5) belong: (i) tan for the active site residues; (ii) green for the residues, which interact with CPR-reductase; (iii) pink for the F-G loop; (iv) yellow for the crystallographic channel of access for ASD; (v) purple for the channel of access for ASD in the presence of the membrane found by some of us;[33] vi) light blue for the D-E loop.

done with single linkage method setting the RMSD cutoff to 0.8 nm.

Calculation of the covariance matrix and the PCA analysis (performed only considering Cα) was done with the *g_covar* and *g_anaeig* tools. All these analysis tools are available in GROMACS 4.5.5.

Schematic plots of ligand/protein interactions were produced using LigPlot+.[37]

Hydrogen bond analysis was done with the *ptraj* module of AMBER12.[38] The distance fluctuation matrix was calculated according to eq 2

$$A_{ij} = \langle (d_{ij} - \langle d_{ij} \rangle) 2 \rangle \tag{2}$$

where d_{ij} is the (time-dependent) distance of the Cα atoms of amino acids i and j, and the brackets indicate the time-average over the trajectory.[39]

We also calculated the Berry index, reporting on the degree of internal structural stability of protein structures according to eq 3[40]

$$\Delta_{B_r} = \frac{2}{N_{r_{cut}}(N_{r_{cut}} - 1)} \sum_i \frac{\sqrt{\langle d_{ij}^2 \rangle - \langle d_{ij} \rangle^2}}{\langle d_{ij} \rangle} \tag{3}$$

where N are all the particles in the system, and d is the distance between the particles i and j.

Binding Free Energy Calculations by MM-GB(PB) SA. The binding free energies of each ligand to each pocket site were calculated with the Molecular Mechanics Poisson–Boltzmann Surface Area (MM-PBSA) and the Molecular Mechanics Generalized Born Surface Area (MM-GBSA), following an established computational protocol.[41,42]

Solute entropy contribution composed by a rototraslational term calculated with classical statistical mechanics and with a vibrational term calculated with the *nmode* module of AMBER12 was estimated considering the solute and a subset of protein residues within a distance of 10 Å from the ligand. This method has been proved to be successful in other systems.[41,43]

The python script MMPBSA.py[44] was used to perform the calculations on 100 and 50 equally spaced frames over the equilibrated trajectory for the ΔH and ΔS part, respectively. MM-GBSA calculations were performed using the Hawkins, Cramer, and Truhlar[45,46] model with parameters described by Tsui and Case;[47] default values were used for all the other settings, while salt concentration was set to 0.1 M.

In MM-PBSA calculations the cavity_surften and cavity_offset values were set to 0.005 and 0.86, respectively. The internal dielectric constant was set to 1.0, while the external one was set to 80.0. A salt concentration of 0.1 M and a probe radius of 1.4 Å were used to determine the dielectric and ion-accessibility coefficients.

Dynamics Based Alignment between HA and Other Membrane Bound Cytochromes. To align HA structure with those of other membrane bound CYP450s we used the ALADYN Web server,[17] which aligns pairs of proteins according to their internal dynamics. Here, HA was aligned with the members of a set of membrane bound cytochromes previously investigated by Otyepka and co-workers,[48] which are associated with metabolism of a large number of clinically used drugs and xenobiotics and for which crystal structures are available.

In particular: CYP1A2 (pdb code: 2HI4[49]), CYP2A6 (pdb code: 1Z10[50]), CYP2C9 (pdb code: 1OG2[51]), CYP2D6 (pdb code: 2F9Q[52]), CYP2E1 (pdb code: 3E6I[53]), CYP3A4 (pdb code 1TQN[54]). These have similar fold to HA and with a sequence identity ranging from 15 to 21% (Table 2).

RESULTS AND DISCUSSION

Identification of Putative Allosteric Sites. Among the five sites alternative to the catalytic one identified by Sitemap we selected only three, which (Table S1 and Figure 2) can be classified as tight-binding sites according to the Halgren definition[21] (a detailed list of the protein residues forming the three selected sites is reported in Table S2).[21] The choice was also dictated by the compatibility of the selected sites with functional and structural details reported in the literature for HA. Namely, we verified if these sites were placed on the access/release pathways identified for ASD entrance/exit in/from the catalytic site in our previous study (Figure 3).[33] Visual inspection revealed that site_1 is close to the most favorable access/release route identified by us.[33]

Then, we also checked whether these peripheral sites were at the HA/CPR interface, so that their engagement by a metabolite could potentially prevent the formation of this adduct

dx.doi.org/10.1021/ci500425y | J. Chem. Inf. Model. 2014, 54, 2856−2868

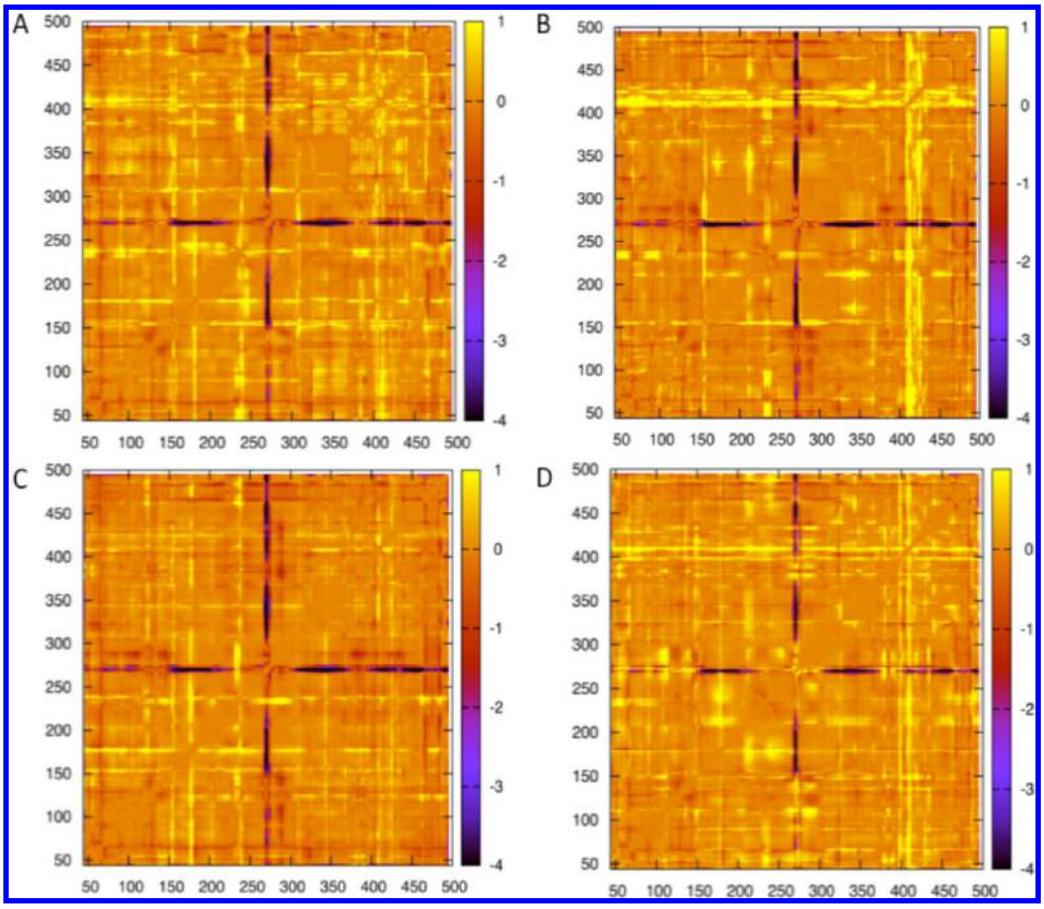

Figure 7. Difference between residue−residue distance fluctuation matrixes for Z-endoxifen (A) and E-endoxifen (B) in site_1 and Z-endoxifen (C) and E-endoxifen (D) in site_3 and that of HA without any inhibitor.[33] The matrices for all other complexes and for HA in water and on a membrane are available as SI. Fluctuation scale is expressed in Å.

Table 4. Barry Indexes Calculated for All the Systems Investigated in This Study[a]

parameter	value
Apo HA $_{\text{(in water)}}$	$(7.92)10^{-3}$
Apo HA$_{\text{(on membrane)}}$	$(9.57)10^{-3}$
Site_1	
E-endoxifen	$(8.74)10^{-3}$
Z-endoxifen	$(9.01)10^{-3}$
E-NDT	$(8.45)10^{-3}$
E-tamoxifen	$(11.0)10^{-3}$
Z-tamoxifen	$(8.43)10^{-3}$
Site_3	
E-endoxifen	$(9.30)10^{-3}$
Z-endoxifen	$(7.11)10^{-3}$
E-NDT E	$(9.20)10^{-3}$
Z-NDT	$(9.67)10^{-3}$
E-tamoxifen	$(11.0)10^{-3}$

[a]For comparison we report BI also for the simulation of HA in water and in membrane.[33]

and in turn hamper the enzymatic activity. In this context, while site_2 lies in the proximity of Lys108 and Lys420 being directly involved in the HA/CPR-reductase recognition,[55] site_3 occupies a peripheral region, which, to the best of our knowledge, is not explicitly involved in any HA functional activity.

E/Z-Endoxifen in the Three Putative Allosteric Sites. Among tamoxifen metabolites (Figure 1), endoxifen showed the strongest noncompetitive inhibition efficacy (Table 1). We thus started our study by predicting its binding mode inside the three selected peripheral sites. We initially docked Z- and E-endoxifen, and, in line with other studies,[56−60] we then performed extensive MD simulations to take into account the mutual ligand protein adaptation and to verify the stability of the predicted endoxifen/HA adducts. After 18 ns of production MD simulation, a first discrimination among the three binding sites was performed by comparing drug/enzyme interaction energies (ΔE_{int}) and by calculating the distance between the protein and ligand centers of mass. In this latter analysis we defined this criterion for the definition of bound vs unbound state of the metabolite: if distance was markedly increasing or significantly changing with respect to that measured in the first MD-frame (more than 4 Å), the drug was considered no longer bound in that site. We selected this distance as the H-bonds keeping the inhibitors bound to the different sites are completely lost after this threshold value and the molecules are no longer bound to HA. According to this criterion we discarded site_2 as E-endoxifen in this site presented the lowest interaction energy with HA (Table S3), while Z-endoxifen dissociated from site_2 already after ∼8 ns of unrestrained MD (Figure S1). After discarding site_2, we docked also the other drugs (i.e., the E/Z-NDT and E/Z-tamoxifen) inside the two remaining peripheral sites, equilibrating the resulting adducts by MD simulations. In this case, Z-NDT in site_1 and Z-tamoxifen in site_3 rapidly dissociated from their respective binding sites (Figure S2), while all other adducts were simulated for an additional 100 ns.

dx.doi.org/10.1021/ci500425y | J. Chem. Inf. Model. 2014, 54, 2856−2868

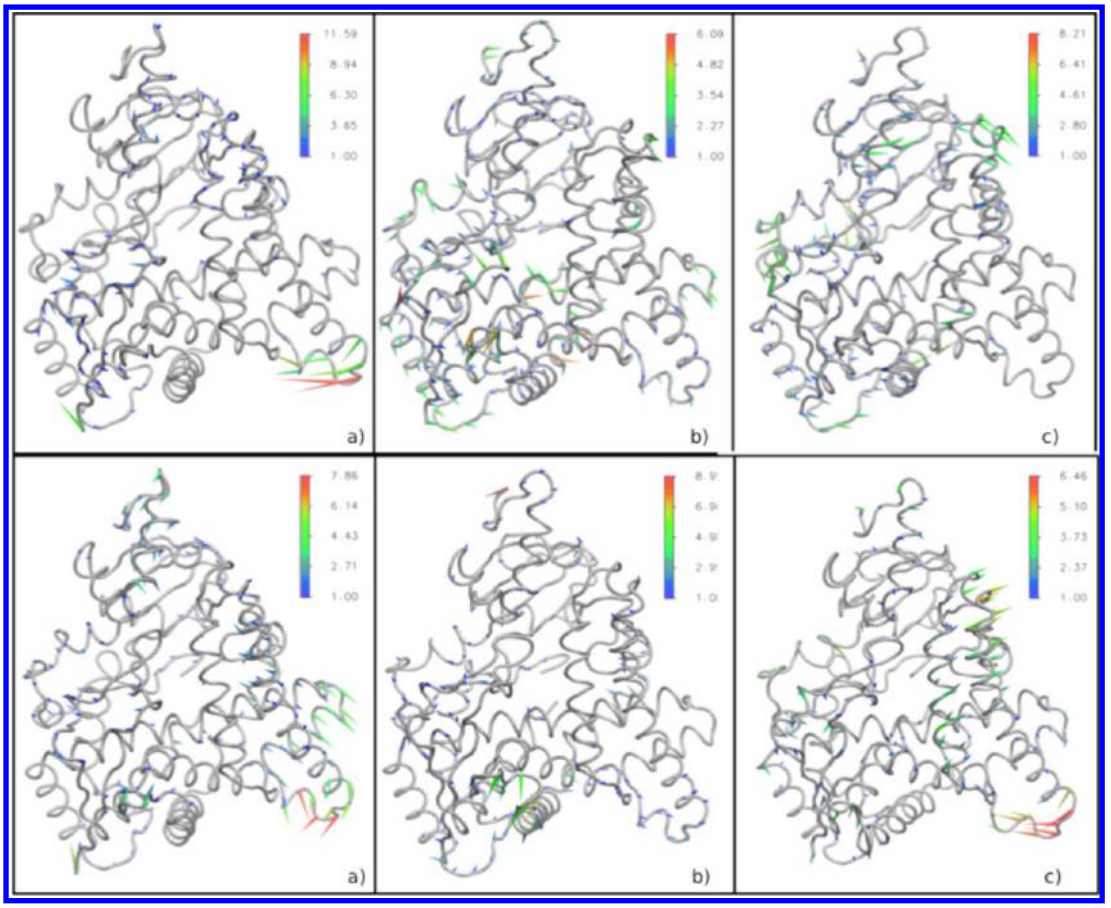

Figure 8. Porcupine plots considering the first PC (first row) and second PC (second row) is here reported for free aromatase (a), Z-endoxifen (b), and E-endoxifen (c) bound in site_1.

We then calculated the binding free energies (ΔG_b) of each ligand to the two sites, as an approximate yet effective indicator of the drug binding affinity for each binding site. Remarkably, the ΔG_b, calculated with the MM-PBSA method, between the drugs in site_3 and the enzyme showed a trend reproducing the experimentally determined IC_{50} (Table 3). In particular, the two endoxifen isomers, which are the most effective noncompetitive inhibitors, were energetically favored over all the other drugs. The same trend is also partially reproduced in the MM-GBSA calculations. However, we have to remark that in both cases the differences are smaller than the standard deviations, which is due to the high flexibility of the allosteric site. Conversely, in site_1, ΔG_b for the different metabolites displayed even an opposite trend with respect to the experimentally determined IC_{50}, with tamoxifen binding with the highest affinity. Most importantly, it is worth noting that the endoxifen isomers, which are the best noncompetitive inhibitors, have the largest binding free energies in site_3, pointing to this as the most likely allosteric site.

The interaction energies between tamoxifen metabolites and HA are in line with the ΔG_b and with the number of hydrogen bonds (H-bonds) established between the drugs and the enzyme (Table S5). E/Z-endoxifen established a substantial number of H-bonds interactions in site_1 (Figure 4) and site_3 (Figure 5). The largest number of H-bonds was detected for Z-endoxifen inside site_1 and site_3, with the occupancy being appreciably higher in site_3 (Table S5). A lower number of H-bonds was instead present in all other drug/HA adducts, due to the reduced number of polar hydrogens of the inhibitors. In site_3, the Z/E-endoxifen occupies a hydrophobic cavity formed by Ala151, Met160, Leu202, Phe203, and Phe278. Z-Endoxifen protrudes more deeply inside the cavity with its phenolic group forming a stable H-bond with Glu281 and its positively charged quaternary nitrogen forming a salt-bridge with Glu274 (Figure 5).

In order to verify if the binding of the inhibitors in the distal sites could influence the affinity of the natural substrate for the catalytic site, we also calculated the ΔE_{int} and between ASD and HA, in the presence or in absence of the E/Z-endoxifen isomers in site_1 and site_3. No marked changes were observed in the ASD/HA interaction energies (ΔE_{int} = −55 (5) kcal/mol) and in the number of ASD/HA H-bonds between the inhibitor bound or free enzyme.[8]

Structural and Dynamical Analysis. We then carried out a structural and internal dynamics analysis of the inhibitor/HA complexes with the aim of investigating whether their binding at the two putative sites could alter the structural of the functional dynamics of HA. Over the last 50 years there has been an intense debate concerning mechanisms of protein allosteric regulation.[61−63] For a long time allosteric modulation was related to a change in protein shape: the ligand (also called allosteric effector) binds to a remote site inducing a conformational change into the orthosteric site (i.e., the binding site of the natural substrate).[64] Recent experimental and theoretical evidence questioned this dogma linking allosteric modulation of proteins also with changes in protein internal dynamics.[65−70] However, the molecular mechanism of allosteric regulation of enzymes is still a highly debated and active research field.[13−16,71−75]

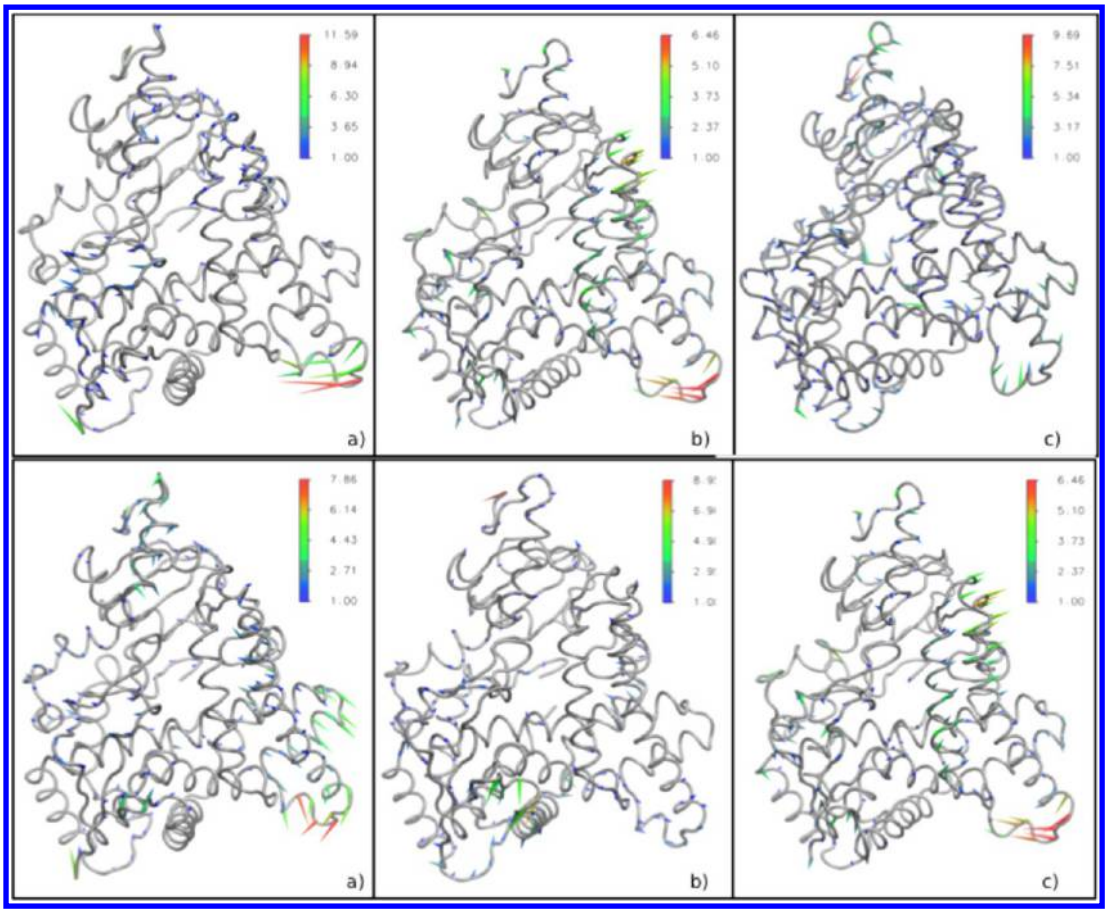

Figure 9. Porcupine plots considering the first PC (first row) and second PC (second row) is here reported for free aromatase (a), Z-endoxifen (b), and E-endoxifen (c) bound in site_3.

Concerning P450 cytochromes a correlation between protein flexibility and substrate selectivity[76−78] was demonstrated, and recent studies elucidated the role of protein flexibility/rigidity on its enzymatic activity.[16]

HA Flexibility. As such, we focused our attention on enzyme flexibility and internal dynamics. In order to evaluate possible perturbative effects on HA structural and dynamical properties induced by the binding of noncompetitive inhibitors, we calculated the RMSF for every HA residue along equilibrated trajectories. Here, we report just the comparison between the two endoxifen stereoisomers, as they were endowed with the most relevant allosteric inhibition effects (Figure 6). RMSF graphs relative to all other adducts are reported in the SI (Figures S3−S4). In particular, we focused on RMSF changes occurring in key-regions, which have been indicated to have a functional role for HA by site directed mutagenesis studies (Table S7). Concerning site_1 (Figure 6A) E/Z-endoxifen similarly influences HA flexibility decreasing the fluctuations of the region between Arg265 and Gly290, roughly corresponding to the G-H′ loop. This loop contributes to a twisting motion believed to be responsible for the breathing of the substrate access channel.[76,79] Conversely, Z-endoxifen increased the mobility of the region surrounding Asp309, which has been proved to play an important role in the enzymatic reaction.[33−35]When E/Z-endoxifen binds to site_3 (Figure 6B), the region of the G-H′ loop (more than 35 Å away from site_3) becomes more rigid, with this effect being more pronounced for the Z isomer. Furthermore, both E/Z-endoxifen slightly increase the flexibility of the region surrounding Asp309. Notably, aiming at evaluating the convergence of RMSF analysis we repeated this analysis considering different parts of the same MD simulation obtaining graphs with the same qualitative meaning (Figure S5).

To complement these results we also performed a residue−residue distance fluctuations analysis over the MD trajectories (Figures 7 and S6−S7). Consistent with RMSF analysis, the visual observation of the fluctuation matrixes evidenced an increased G-H′ loop rigidity in the presence of endoxifen in both peripheral sites.

To estimate more quantitatively the global protein flexibility, we also calculated the Berry Index[40] (BI) (a qualitative index of the thermal disorder)[40] for all the adducts (Table 4). The BIs confirmed the Z-endoxifen/HA adduct, with the inhibitor bound inside site_3, as the most rigid among those considered in the study, while the HA/E-tamoxifen complex showed the lowest impact on protein rigidification, in line with its low efficacy as a noncompetitive inhibitor. For the sake of comparison we also calculated the BI of HA without allosteric modulators considering both simulations in water and with the membrane environment.[33] Remarkably, the HA embedded in the membrane is characterized by a large BI,[33] pointing once more to a significant role of internal dynamics for HA enzymatic activity.

Principal Component Analysis. We then performed Principal Component Analysis (PCA) for E/Z endoxifen bound in site_ 1 and site_3 as compared to that of free HA. To visualize the differences between the two adducts at glance we report the first two principal components (PC) for each system as a porcupine plot (Figures 8 and 9). Considering the

dx.doi.org/10.1021/ci500425y | J. Chem. Inf. Model. 2014, 54, 2856−2868

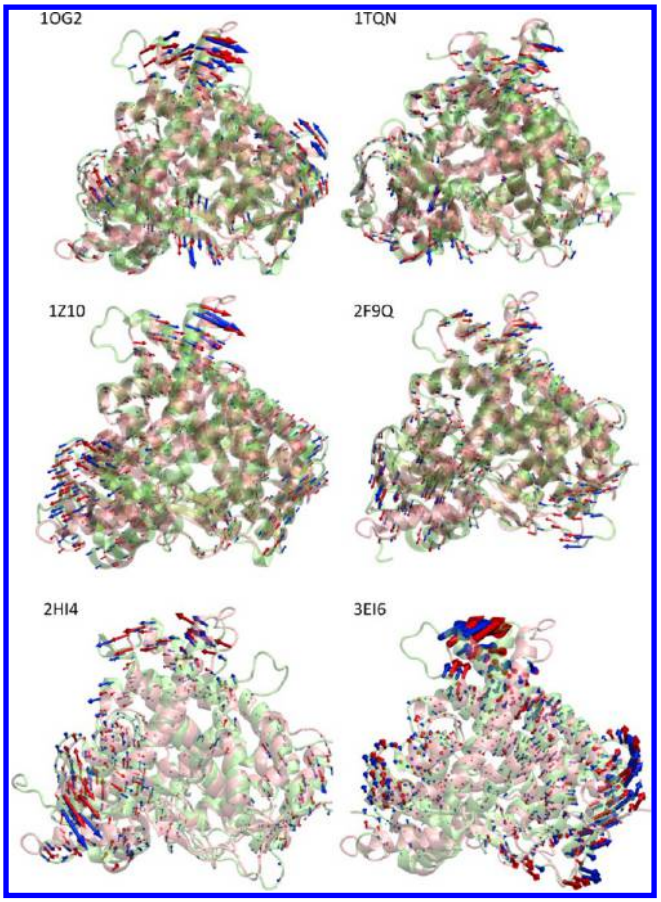

Figure 10. Dynamic based alignment between HA and six membrane bound cytochromes. HA structure is always depicted in pink and the slow functional motion is indicated by red arrows, while the aligned structure is in green with the corresponding motion indicated by blue arrows.

binding at site_3 (Figure 9) we observe that the intense motion of the G-H′ loop present in free HA when simulated in pure water and on the membrane surface (Figure S8) is significantly reduced upon E-endoxifen binding and almost completely dumped in the presence of Z-endoxifen, consistently with RMSF analysis. A similar dumping effect is also observed upon binding of both E/Z-endoxifen in site_1 (Figure 8), although less pronounced.

PCA in Other Human CYPs. CYP450 is a major superfamily of enzymes involved in the metabolism of diverse variety xenobiotics. Some drawbacks are associated with CYP450s enzymatic activity (reduction of bioavailability of drugs, safety or efficacy of drugs; production of potentially carcinogenic or toxic compounds), such that the modulation of their enzymatic activity via inhibition is of the outmost interest.[80,81]

Recently Micheletti and co-workers proposed a computational method (ALADYN)[17] to perform protein alignment considering protein internal dynamics and large scale movements. Herein, we used ALADYN to align HA structure with those of other selected membrane bound CYPs involved in similar oxidative reactions associated with xenobiotics metabolisms.[50−52,54] It is in fact well-known that slow time-scale motions are at the basis of CYP450 function and ligand recognition.[48,77,82] For all CYPs considered (with a sequence identity ranging between 15 and 21%), we obtained a satisfactory alignment (Table 2), being the global RMSD < 3 Å, along with a significant correspondence of the low energy modes (highlighted by a root-mean-square inner product (RMSIP) near 0.90).

Visual inspection of the resulting alignments as well as of the first four low energy motions identified a similar collective motion corresponding to PC1/PC2 of free HA (Figure 10). Not surprisingly, a similar motion, contributing to substrate uptake efficiency, has a key role for the HA enzymatic activity.[12] Thus, this dynamics-based alignment between a sterodoigenic CYP450 and other drug metabolizing CYP450s reveals common functional motions, suggesting potential common pathways of inhibition based on allosteric modulation, which is so far little explored.

SUMMARY AND CONCLUSIONS

In this study, we develop and use a new computational protocol to investigate at the atomistic level of detail the mechanisms of HA allosteric modulation exerted by tamoxifen metabolites.[8] After having identified three possible binding sites, we performed systematic docking studies and extensive MD simulations (the total simulation time exceeded 1.2 μs) to verify the stability of the predicted complexes. Two sites were selected for further analysis on the basis of the relative stability of inhibitor binding. Interestingly a qualitative correspondence was observed between the binding free energies of various tamoxifen metabolites in site_3, which correlates with the experimentally determined IC50. Moreover, the binding free energies of the most effective noncompetitive inhibitors (the Z and E-endoxifen isomers) result in being more negative in this site. Additional analyses (RMSF, PCA, and residue−residue distance fluctuations) were permitted to shed light on how the two most effective noncompetitive inhibitors alter the G-H′ loop mobility when they are bound in either site_1 or site_3, with protein rigidity being maximal upon Z-endoxifen binding in site_3. Since a twisting motion of the G-H′ loop is believed to contribute to the breathing of the substrate access channel to the active site,[12] damping of this motion is clearly important to modulate the steroidogenesis activity of HA, providing a rationale for the experimentally observed allosteric inhibition mechanism.

From the medicinal chemistry point of view, identification of an allosteric binding site by which modulating HA enzymatic activity could be significantly important for: (1) development of more selective allosteric inhibitors aiming at overcoming the side effects of anticancer drugs targeting HA and (2) the comprehension of the molecular mechanism connected with the raising of undesirable side effects of these currently used anticancer drugs. In this context, we envisage that (pan)inhibitors could be designed to modulate both the activity of HA and of estrogen receptors to treat breast cancers.

Besides this very important finding, we also observe that a collective motion similar to that inhibited in HA is also present in the other six selected CYP450s, suggesting that the same allosteric modulation pathway may be exploited also in other CYP450. Since some P450-catalyzed reactions can transform relatively inert compounds into genotoxic metabolites, which can promote mutagenesis and cancer, our results offer also new possible routes to explore in the drug design projects aiming at chemoprevention and/or chemoprotection.

ASSOCIATED CONTENT

Supporting Information

Additional details about Sitemap calculation; a list of residues forming the three putative sites considered in the work; interaction energies calculated over MD simulations; H-bond

dx.doi.org/10.1021/ci500425y | J. Chem. Inf. Model. 2014, 54, 2856−2868

analysis over MD simulations; summary of HA residues targeted by mutagenesis studies; RMSD, RMSF, distance fluctuation matrixes, and porcupine plots not shown in the main text. This material is available free of charge via the Internet at http://pubs.acs.org.

AUTHOR INFORMATION

Corresponding Authors

*E-mail: alessandra.magistrato@sissa.it.
*E-mail: g.colombo@icrm.cnr.it.

Author Contributions

⊥J.S and M.B. equally contributed to this work.

Notes

The authors declare no competing financial interest.

ACKNOWLEDGMENTS

We acknowledge the CINECA and the Regione Lombardia award under the LISA initiative, for the availability of high performance computing resources and support. Support was also received from AIRC (Associazione Italiana Ricerca sul Cancro), Grant IG. 11775 to G.C. and by the Italian Ministry of Education and Research through the Flagship (PB05) "InterOmics".

REFERENCES

(1) Di Nardo, G.; Gilardi, G. Human aromatase: perspectives in biochemistry and biotechnology. *Biotechnol. Appl. Biochem.* **2013**, *60*, 92−101.

(2) Banting, L.; Ahmed, S. Aromatase: the enzyme and its inhibition. *Anticancer Agents Med. Chem.* **2009**, *9*, 627−641.

(3) Akhtar, M.; Wright, J. N.; Lee-Robichaud, P. A review of mechanistic studies on aromatase (CYP19) and 17Œ±-hydroxylase-17,20-lyase (CYP17). *J. Steroid Biochem. Mol. Biol.* **2010**, *125*, 2−12.

(4) Liang, J.; Shang, Y. Estrogen and Cancer. *Annu. Rev. Physiol.* **2013**, *75*, 225−240.

(5) Hutchinson, L. Breast cancer: Challenges, controversies, breakthroughs. *Nat. Rev. Clin. Oncol.* **2010**, *7*, 669−670.

(6) Miller, W.; Larionov, A. Understanding the mechanisms of aromatase inhibitor resistance. *Breast Cancer Res.* **2012**, *14*, 201−213.

(7) Favia, A. D.; Nicolotti, O.; Stefanachi, A.; Leonetti, F.; Carotti, A. Computational methods for the design of potent aromatase inhibitors. *Expert Opin. Drug Discovery* **2013**, *8*, 395−409.

(8) Lu, W. J.; Desta, Z.; Flockhart, D. A. Tamoxifen metabolites as active inhibitors of aromatase in the treatment of breast cancer. *Breast Cancer Res. Treat.* **2011**, 473−481.

(9) Lu, W. J.; Xu, C.; Pei, Z.; Mayhoub, A. S.; Cushman, M.; Flockhart, D. A. The tamoxifen metabolite norendoxifen is a potent and selective inhibitor of aromatase (CYP19) and a potential lead compound for novel therapeutic agents. *Breast Cancer Res. Treat.* **2012**, *133*, 99−109.

(10) Lv, W.; Liu, J.; Lu, D.; Flockhart, D. A.; Cushman, M. Synthesis of Mixed (E,Z)-, (E)-, and (Z)-Norendoxifen with Dual Aromatase Inhibitory and Estrogen Receptor Modulatory Activities. *J. Med. Chem.* **2013**, *56*, 4611−4618.

(11) Liu, J.; Flockhart, P. J.; Lu, D.; Lv, W.; Lu, W. J.; Han, X.; Cushman, M.; Flockhart, D. A. Inhibition of cytochrome p450 enzymes by the e- and z-isomers of norendoxifen. *Drug Metab. Dispos.* **2013**, *41*, 1715−1720.

(12) Lo, J.; Di Nardo, G.; Griswold, J.; Egbuta, C.; Jiang, W.; Gilardi, G.; Ghosh, D. Structural basis for the functional roles of critical residues in human cytochrome p450 aromatase. *Biochemistry* **2013**, *52*, 5821−5829.

(13) Sineva, E. V.; Rumfeldt, J. A. O.; Halpert, J. R.; Davydov, D. R. A large-scale allosteric transition in cytochrome P450 3A4 revealed by luminescence resonance energy transfer (LRET). *PLoS One* **2013**, *8*, e83898.

(14) Zhang, H.; Gay, S. C.; Shah, M.; Foroozesh, M.; Liu, J.; Osawa, Y.; Zhang, Q.; Stout, C. D.; Halpert, J. R.; Hollenberg, P. F. Potent mechanism-based inactivation of cytochrome P450 2B4 by 9-ethynylphenanthrene: implications for allosteric modulation of cytochrome P450 catalysis. *Biochemistry* **2013**, *52*, 355−364.

(15) Estrada, D. F.; Laurence, J. S.; Scott, E. E. Substrate-modulated cytochrome P450 17A1 and cytochrome b5 interactions revealed by NMR. *J. Biol. Chem.* **2013**, *288*, 17008−17018.

(16) Childers, W. K.; Harrelson, J. P. Allosteric Modulation of Substrate Motion in Cytochrome P450 3A4-Mediated Xylene Oxidation. *Biochemistry* **2014**, *53*, 1018−1028.

(17) Potestio, R.; Aleksiev, T.; Pontiggia, F.; Cozzini, S.; Micheletti, C. ALADYN: a web server for aligning proteins by matching their large-scale motion. *Nucleic Acids Res.* **2010**, *38*, W41−W45.

(18) Ghosh, D.; Griswold, J.; Erman, M.; Pangborn, W. Structural basis for androgen specificity and oestrogen synthesis in human aromatase. *Nature* **2009**, *457*, 219−223.

(19) *Maestro*, version 9.2; Schrödinger, LLC: New York, NY, 2011.

(20) Halgren, T. New Method for Fast and Accurate Binding-site Identification and Analysis. *Chem. Biol. Drug Des.* **2007**, *69*, 146−148.

(21) Halgren, T. A. Identifying and Characterizing Binding Sites and Assessing Druggability. *J. Chem. Inf. Model.* **2009**, *49*, 377−389.

(22) Friesner, R. A.; Banks, J. L.; Murphy, R. B.; Halgren, T. A.; Klicic, J. J.; Mainz, D. T.; Repasky, M. P.; Knoll, E. H.; Shelley, M.; Perry, J. K.; Shaw, D. E.; Francis, P.; Shenkin, P. S. Glide: a new approach for rapid, accurate docking and scoring. 1. Method and assessment of docking accuracy. *J. Med. Chem.* **2004**, *47*, 1739−1749.

(23) Friesner, R. A.; Murphy, R. B.; Repasky, M. P.; Frye, L. L.; Greenwood, J. R.; Halgren, T. A.; Sanschagrin, P. C.; Mainz, D. T. Extra precision glide: docking and scoring incorporating a model of hydrophobic enclosure for protein-ligand complexes. *J. Med. Chem.* **2006**, *49*, 6177−6196.

(24) Suite 2012: *Glide*, version 5.8; Schrodinger, LLC: New York, NY, 2012.

(25) Hess, B.; Kutzner, C.; van der Spoel, D.; Lindahl, E. GROMACS 4: Algorithms for Highly Efficient, Load-Balanced, and Scalable Molecular Simulation. *J. Chem. Theory Comput.* **2008**, *4*, 435−447.

(26) Hess, B.; Bekker, H.; Berendsen, H. J. C.; Fraaije, J. G. E. M. LINCS: A linear constraint solver for molecular simulations. *J. Comput. Chem.* **1997**, *18*, 1463−1472.

(27) Hoover, W. G. Canonical dynamics: Equilibrium phase-space distributions. *Phys. Rev. A* **1985**, *31*, 1695−1697.

(28) Parrinello, M.; Rahman, A. Polymorphic transitions in single crystals: A new molecular dynamics method. *J. Appl. Phys.* **1981**, *52*, 7182−7190.

(29) Jorgensen, W. L.; Chandrasekhar, J.; Madura, J. D.; Impey, R. W.; Klein, L. M. Comparison of simple potential functions for simulating liquid water. *J. Chem. Phys.* **1983**, *79*, 926−935.

(30) Aaqvist, J. Ion-water interaction potentials derived from free energy perturbation simulations. *J. Chem. Phys.* **1990**, *94*, 8021−8024.

(31) Shahrokh, K.; Orendt, A.; Yost, G. S.; Cheatham, T. E. Quantum mechanically derived AMBER-compatible heme parameters for various states of the cytochrome P450 catalytic cycle. *J. Comput. Chem.* **2012**, *33*, 119−133.

(32) Wang, J.; Wolf, R. M.; Caldwell, J. W.; Kollman, P. A.; Case, D. A. Development and testing of a general amber force field. *J. Comput. Chem.* **2004**, *25*, 1157−1174.

(33) Sgrignani, J.; Magistrato, A. Influence of the membrane lipophilic environment on the structure and on the substrate access/egress routes of the human aromatase enzyme. A computational study. *J. Chem. Inf. Model.* **2012**, *52*, 1595−1606.

(34) Park, J.; Czapla, L.; Amaro, R. E. Molecular simulations of aromatase reveal new insights into the mechanism of ligand binding. *J. Chem. Inf. Model.* **2013**, *53*, 2047−2056.

(35) Sen, K.; Hackett, J. C. Coupled electron transfer and proton hopping in the final step of CYP19-catalyzed androgen aromatization. *Biochemistry* **2012**, *51*, 3039−3049.

(36) Humphrey, W.; Dalke, A.; Schulten, K. VMD: visual molecular dynamics. *J. Mol. Graph.* **1996**, *14*, 33−38.

(37) Laskowski, R. A.; Swindells, M. B. LigPlot+: Multiple Ligand−Protein Interaction Diagrams for Drug Discovery. *J. Chem. Inf. Model.* **2011**, *51*, 2778−2786.
(38) Case, D. A.; Darden, T. A.; Cheatham, T. E., III; Simmerling, C. L.; Wang, J.; Duke, R. E.; Luo, R.; Walker, R. C.; Zhang, W.; Merz, K. M.; Roberts, B.; Wang, B.; Hayik, S.; Roitberg, A.; Seabra, G.; Kolossvary, I.; Wong, K. F.; Paesani, F.; Vanicek, J.; Liu, J.; Wu, X.; Brozell, S. R.; Steinbrecher, T.; Gohlke, H.; Cai, Q.; Ye, X.; Wang, J.; Hsieh, M.-J.; Cui, G.; Roe, D. R.; Mathews, D. H.; Seetin, M. G.; Sagui, C.; Babin, V.; Luchko, T.; Gusarov, S.; Kovalenko, A.; Kollman, P. A. In *AMBER11*; University of California: 2010.
(39) Chiappori, F.; Merelli, I.; Colombo, G.; Milanesi, L.; Morra, G. Molecular mechanism of allosteric communication in Hsp70 revealed by molecular dynamics simulations. *PLoS Comput. Biol.* **2012**, *8*, e1002844.
(40) Zhou, Y.; Karplus, M.; Ball, K. D.; Berry, R. S. The distance fluctuation criterion for melting: Comparison of square-well and Morse potential models for clusters and homopolymers. *J. Chem. Phys.* **2002**, *116*, 2323−2329.
(41) Vargiu, A. V.; Nikaido, H. Multidrug binding properties of the AcrB efflux pump characterized by molecular dynamics simulations. *Proc. Natl. Acad. Sci. U. S. A.* **2012**, *109*, 20637−20642.
(42) Vargiu, A. V.; Magistrato, A. Detecting DNA Mismatches with Metallo-Insertors: A Molecular Simulation Study. *Inorg. Chem.* **2012**, *51*, 2046−2057.
(43) Kongsted, J.; Ryde, U. An improved method to predict the entropy term with the MM/PBSA approach. *J. Comput.-Aided Mol. Des.* **2009**, *23*, 63−71.
(44) Miller, B. R.; McGee, T. D.; Swails, J. M.; Homeyer, N.; Gohlke, H.; Roitberg, A. E. MMPBSA.py: An Efficient Program for End-State Free Energy Calculations. *J. Chem. Theory Comput.* **2012**, *8*, 3314−3321.
(45) Hawkins, G. D.; Cramer, C. J.; Truhlar, D. G. Parametrized Models of Aqueous Free Energies of Solvation Based on Pairwise Descreening of Solute Atomic Charges from a Dielectric Medium. *J. Phys. Chem.* **1996**, *100*, 19824−19839.
(46) Gaillard, T.; Case, D. A. Evaluation of DNA Force Fields in Implicit Solvation. *J. Chem. Theory Comput.* **2011**, *7*, 3181−3198.
(47) Tsui, V.; Case, D. A. Theory and applications of the generalized Born solvation model in macromolecular simulations. *Biopolymers* **2000**, *56*, 275−91.
(48) Berka, K.; Paloncyova, M.; Anzenbacher, P.; Otyepka, M. Behavior of human cytochromes P450 on lipid membranes. *J. Phys. Chem. B* **2013**, *117*, 11556−64.
(49) Sansen, S.; Yano, J. K.; Reynald, R. L.; Schoch, G. A.; Griffin, K. J.; Stout, C. D.; Johnson, E. F. Adaptations for the oxidation of polycyclic aromatic hydrocarbons exhibited by the structure of human P450 1A2. *J. Biol. Chem.* **2007**, *282*, 14348−55.
(50) Yano, J. K.; Hsu, M. H.; Griffin, K. J.; Stout, C. D.; Johnson, E. F. Structures of human microsomal cytochrome P450 2A6 complexed with coumarin and methoxsalen. *Nat. Struct. Mol. Biol.* **2005**, *12*, 822−3.
(51) Williams, P. A.; Cosme, J.; Ward, A.; Angove, H. C.; Matak Vinkovic, D.; Jhoti, H. Crystal structure of human cytochrome P450 2C9 with bound warfarin. *Nature* **2003**, *424*, 464−8.
(52) Rowland, P.; Blaney, F. E.; Smyth, M. G.; Jones, J. J.; Leydon, V. R.; Oxbrow, A. K.; Lewis, C. J.; Tennant, M. G.; Modi, S.; Eggleston, D. S.; Chenery, R. J.; Bridges, A. M. Crystal structure of human cytochrome P450 2D6. *J. Biol. Chem.* **2006**, *281*, 7614−22.
(53) Porubsky, P. R.; Meneely, K. M.; Scott, E. E. Structures of human cytochrome P-450 2E1. Insights into the binding of inhibitors and both small molecular weight and fatty acid substrates. *J. Biol. Chem.* **2008**, *283*, 33698−707.
(54) Yano, J. K.; Wester, M. R.; Schoch, G. A.; Griffin, K. J.; Stout, C. D.; Johnson, E. F. The structure of human microsomal cytochrome P450 3A4 determined by X-ray crystallography to 2.05-A resolution. *J. Biol. Chem.* **2004**, *279*, 38091−4.
(55) Hong, Y.; Li, H.; Ye, J.; Miki, Y.; Yuan, Y.-C.; Sasano, H.; Evans, D. B.; Chen, S. Epitope Characterization of an Aromatase Monoclonal Antibody Suitable for the Assessment of Intratumoral Aromatase Activity. *PLoS One* **2009**, *4*, e8050.
(56) Alonso, H.; Bliznyuk, A. A.; Gready, J. E. Combining docking and molecular dynamic simulations in drug design. *Med. Res. Rev.* **2006**, *26*, 531−568.
(57) Marco, E.; Gago, F. Overcoming the Inadequacies or Limitations of Experimental Structures as Drug Targets by Using Computational Modeling Tools and Molecular Dynamics Simulations. *ChemMedChem.* **2007**, *2*, 1388−1401.
(58) Sgrignani, J.; Bonaccini, C.; Grazioso, G.; Chioccioli, M.; Cavalli, A.; Gratteri, P. Insights into docking and scoring neuronal alpha4beta2 nicotinic receptor agonists using molecular dynamics simulations and QM/MM calculations. *J. Comput. Chem.* **2009**, *30*, 2443−2454.
(59) Durrant, J. D.; McCammon, J. A. Molecular dynamics simulations and drug discovery. *BMC Biol.* **2011**, *9*, 71−80.
(60) Sgrignani, J.; Magistrato, A. First-principles modeling of biological systems and structure-based drug-design. *Curr. Comput.-Aided Drug Des.* **2013**, *9*, 15−34.
(61) Nussinov, R.; Tsai, C.-J. Allostery in Disease and in Drug Discovery. *Cell* **2013**, *153*, 293−305.
(62) Tsai, C.-J.; Nussinov, R. A unified view of "how allostery works". *PLoS Comput. Biol.* **2014**, *10*, e1003394.
(63) Goodey, N. M.; Benkovic, S. J. Allosteric regulation and catalysis emerge via a common route. *Nat. Chem. Biol.* **2008**, *4*, 474−482.
(64) Tsai, C.-J.; del Sol, A.; Nussinov, R. Allostery: absence of a change in shape does not imply that allostery is not at play. *J. Mol. Biol.* **2008**, *378*, 1−11.
(65) Frederick, K. K.; Marlow, M. S.; Valentine, K. G.; Wand, A. J. Conformational entropy in molecular recognition by proteins. *Nature* **2007**, *448*, 325−329.
(66) Veglia, G.; Cembran, A. Role of conformational entropy in the activity and regulation of the catalytic subunit of protein kinase A. *FEBS J.* **2013**, *280*, 5608−5615.
(67) Tzeng, S.-R.; Kalodimos, C. G. Protein dynamics and allostery: an NMR view. *Curr. Opin. Struct. Biol.* **2011**, *21*, 62−67.
(68) Kokkinidis, M.; Glykos, N. M.; Fadouloglou, V. E. Chapter 7 - Protein Flexibility and Enzymatic Catalysis. In *Advances in Protein Chemistry and Structural Biology*; Christo, C., Tatyana, K.-C., Eds.; Academic Press: 2012; Vol. *87*, pp 181−218.
(69) McDonald, L. R.; Whitley, M. J.; Boyer, J. A.; Lee, A. L. Colocalization of Fast and Slow Timescale Dynamics in the Allosteric Signaling Protein CheY. *J. Mol. Biol.* **2013**, *425*, 2372−2381.
(70) He, Y.; Chen, J. Y.; Knab, J. R.; Zheng, W.; Markelz, A. G. Evidence of Protein Collective Motions on the Picosecond Timescale. *Biophys. J.* **2011**, *100*, 1058−1065.
(71) Daniel, R. M.; Dunn, R. V.; Finney, J. L.; Smith, J. C. The role of dynamics in enzyme activity. *Annu. Rev. Biophys. Biomol. Struct.* **2003**, *32*, 69−92.
(72) Thielges, M. C.; Chung, J. K.; Fayer, M. D. Protein dynamics in cytochrome P450 molecular recognition and substrate specificity using 2D IR vibrational echo spectroscopy. *J. Am. Chem. Soc.* **2011**, *133*, 3995−4004.
(73) Klinman, J. P.; Kohen, A. Hydrogen Tunneling Links Protein Dynamics to Enzyme Catalysis. *Annu. Rev. Biochem.* **2013**, *82*, 471−496.
(74) Loveridge, E. J.; Behiry, E. M.; Guo, J.; Allemann, R. K. Evidence that a 'dynamic knockout' in Escherichia coli dihydrofolate reductase does not affect the chemical step of catalysis. *Nat. Chem.* **2012**, *4*, 292−297.
(75) Bhabha, G.; Lee, J.; Ekiert, D. C.; Gam, J.; Wilson, I. A.; Dyson, H. J.; Benkovic, S. J.; Wright, P. E. A dynamic knockout reveals that conformational fluctuations influence the chemical step of enzyme catalysis. *Science* **2011**, *332*, 234−238.
(76) Di Nardo, G.; Breitner, M.; Sadeghi, S. J.; CastrignanÚ, S.; Mei, G.; Di Venere, A.; Nicolai, E.; Allegra, P.; Gilardi, G. Dynamics and Flexibility of Human Aromatase Probed by FTIR and Time Resolved Fluorescence Spectroscopy. *PLoS One* **2013**, *8*, e82118.

(77) Otyepka, M.; Berka, K.; Anzenbacher, P. Is there a relationship between the substrate preferences and structural flexibility of cytochromes P450? *Curr. Drug Metab.* **2012**, *13*, 130−142.
(78) SkopalÌk, J.; Anzenbacher, P.; Otyepka, M. Flexibility of human cytochromes P450: molecular dynamics reveals differences between CYPs 3A4, 2C9, and 2A6, which correlate with their substrate preferences. *J. Phys. Chem. B* **2008**, *112*, 8165−8173.
(79) Jiang, W.; Ghosh, D. Motion and flexibility in human cytochrome p450 aromatase. *PLoS One* **2012**, *7*, e32565.
(80) Hari Kumar, K. B.; Kuttan, R. Inhibition of drug metabolizing enzymes (cytochrome P450) in vitro as well as in vivo by Phyllanthus amarus. *Biol. Pharm. Bull.* **2006**, *29*, 1310−1313.
(81) Badal, S.; Delgoda, R. Role of the modulation of CYP1A1 expression and activity in chemoprevention: A mini review. *J. Appl. Toxicol.* **2014**, *34*, 743−753.
(82) Hendrychov, T.; Anzenbacherov, E.; Hudeček, J.; Skopalìk, J.; Lange, R.; Hildebrandt, P.; Otyepka, M.; Anzenbacher, P. Flexibility of human cytochrome P450 enzymes: molecular dynamics and spectroscopy reveal important function-related variations. *Biochim. Biophys. Acta* **2011**, *1814*, 58−68.